An expression for the dynamic stability of blunt slender elliptic bodies in hypersonic flow

M. Khalid
mkholid@kau.edu.sa
K. A. Juhany
King Abdul Aziz University
Jeddah
Saudi Arabia

ABSTRACT

Dynamic stability data on axially symmetric pointed and blunt cones, parabolic profiles and other ogive and blunt cylindrical shapes is readily available in literature; the dynamic stability on elliptic blunt paraboloids has not been studied at any great lengths in the past. Both numerical and experimental results are scarce. The present paper uses the shock expansion method to obtain the unsteady pressure distribution on blunt elliptic conical bodies at small angles-of-attack. The resulting unsteady pressure distribution is suitably integrated over the surface of the elliptic body to obtain appropriate analytic expressions for static and dynamic stability. Owing to scarcity of meaningful numerical or measured data for elliptic bodies, the results are compared in qualitative terms against published dynamic stability data on pointed elliptical cones or other axisymmetric blunt cones.

NOMENCLATURE

a	major axis for the elliptic cross section
b	minor axis for the elliptic cross section
c	body length
C_∞	constant of proportionality between viscosity and temperature
C_p	pressure coefficient $\frac{2}{\gamma M_\infty^2}\left\{\frac{p}{p_\infty}-1\right\}$

Paper No. 4017. Manuscript received 10 June 2013, revised version received 21 March 2014, accepted 24 March 2014.

https://doi.org/10.1017/S0001924000009751 Published online by Cambridge University Press

$$Cm_{\dot{\theta}} = Cm_q + Cm_{\dot{\alpha}} = \frac{2V_\infty}{c}\left(\frac{\partial Cm}{\partial \dot{\theta}}\right)_{\ddot{z}=0,\dot{\alpha}=0,\alpha_e\to\alpha,\dot{\theta}\to 0}$$

$$Cm_\alpha = \frac{V_\infty}{c}\left(\frac{\partial Cm}{\partial \alpha}\right)_{q=0,\ddot{z}=0,\dot{\alpha}=0,\alpha_e\to\alpha}$$

Cos(n,x), Cos (n,y), Cos (n,z) direction cosines in x, y, z directions

$h(x,t)$ instantaneous height of a point on the body

x,y,z axes direction (See Fig. 1)

s distance measure along the curved elliptic body from origin

S_{max} max value of s

t time constant

t_0 time instant when a fluid element passes the body apex

q angular velocity of body about pitch axis, $x = x_0$ (positive in nose up direction)

R Reynolds number

V velocity

$\overline{V}_N$ velocity conditions at the apex

M_N Mach number conditions at the apex

$X0$, $x0$ axis of oscillation position

γ specific heat ratio, gas constant = 1·4

z lateral translation

α angle-of-attack

β yaw angle

Δ_{ep} change in angle of inclination of tangent to (projected) streamline (path line) of a particular fluid element between vertex and point (x, $R(x)$, φ) on body surface, measured in osculating plane of reference

$\theta_o(x)$ local angle of inclination of body surface to axis of symmetry

θ_N slope of the body at the designated apex

θ pitch angle

φ azimuthal direction (360-θ), with θ defined in Fig. 1

$\tau(x)$ function of x occurring in transformation to (local) flow fixed co-ordinates, $t = \tau(x)$

χ $\chi(x,y,z)$ three dimension representation of the ellipsoid geometry

∞ free stream condition

1.0 INTRODUCTION

The aerodynamicists have from time to time devised a number of analytical methods to compute hypersonic flow field past axi-symmetric conical bodies. For pointed nosed bodies, the solutions are comparatively easier as the flow along the body can be computed directly if the shock remains attached to the body. However, exceedingly high temperature effects force the material to ablate from near the nose, causing undesired asymmetry of the nose profile. To prevent this and the need to alleviate high heat transfer rates near a pointed nose, has necessitated the fore body to have a blunter spherical profile forcing the shock to remain detached from the nose. The flow field past a blunt nosed conical body is somewhat more complex than the flow past a pointed body. As far as the sharp edged cones, wedges and other pointed bodies of revolution are concerned, numerous parametric studies have been reported for a range of hypersonic Mach numbers. Hui[1-3] and Hemdan[4] have provided an account of some of this earlier theoretical work on wedges, cones, aerofoils, delta and carot wings. For experimental data Hobs[5] Welsh *et al*[6] and Brong[7] have provided a set of data on measurements recorded for a

https://doi.org/10.1017/S0001924000009751 Published online by Cambridge University Press

10° half-angle cone. Rie *et al*[8], not only provided the first CFD based approximations based on Euler equations but also presented some interesting comparisons of their predictions with measurements.

These earlier theories had used perturbation methods based on potential flow, small disturbance theory due to van Dyke[9], unsteady Newtonian-Buseman method[10], tangent wedge/cone method[11] or the piston theory, which was first proposed by Lighthill[12] in application to oscillating aerofoils some 60 years ago. Ashley and Zartarian[13] discuss piston theory while providing a number of examples of the application of piston theory to some specific problems. For blunt bodies of revolution, the flow near the nose was complicated by the detachment of the shock from the body. Khalid and East[14] had used the blast wave analogy due to Taylor[15] and Chernyi[16] to model the steady flow field which was then perturbed using the shock expansion method to obtain the unsteady flow field leading to stability derivatives. Later they extended this work to cover higher angles of attack for both pointed[17] and blunt nose applications[18], as well as the inclusion of the viscous effects[19]. Ramussen and Lee[20] provided exact flow field solution for the elliptic pointed cone and Ericsson[21] has used the embedded Newtonian methods at length to provide good empirical estimates for predicting dynamic stability derivatives for missile type projectiles.

The dynamic stability results on blunt elliptic shapes are very scarce. The present method uses the classic modified Newtonian methods to obtain an analytic expression for the pressure distribution on a blunt elliptic body at small but finite angles of attack. Assuming that the flow remains conical, the steady pressure distribution is then perturbed subject to specific pitching or translational motion schedule. The assumption of conical flow for elliptic cones is quite valid, as the individual streamline away from the influence of the blunt nose remains linear unlike the corresponding streamlines from a blunt ogive or a power law body where the body thickness continues to expand axially in a non-linear fashion.

The assumption of conical flow must however be treated carefully in presence of the blunt nose which is bound to introduce strong 3D effects and other viscous interaction near the nose region. Hayes and Probstein[22] have shown that for bodies of revolution, the effect in region l downstream owing to nose thickness d_n, is related to an interaction parameter $\bar{\chi}$ through the relationships:

$$\frac{1}{d_n} \sim \frac{M_\infty^2}{\bar{\chi}}$$

where,

$$\bar{\chi} \sim M_\infty^4 \, C_\infty / R_{dn}$$

Betram[23]and Kendall[24] have confirmed that for flows with strong interaction parameter, $\bar{\chi} > 3$, which would be the case for hypersonic flows with $M_\infty > 7$, the bluntness induced effects are limited to very small region $d_n \leq 1$, close to the nose region. Lees[25] as well as the experimental results shown later, confirm that large pressure gradients on bodies of revolution due to bluntness are limited to regions very close to the nose.

The resulting unsteady flow field is the appropriately integrated around the body to obtain the dynamic stability derivatives.

2.0 ANALYTIC MODELING

In order to account for the blunting effects, an elliptic cross section was selected which remained blunt near the stagnation region, unlike the elliptic geometries which end up in a point singularity at the nose inviting shock attachment to the body. Figure 1 as described in Ref. 26 was then selected

https://doi.org/10.1017/S0001924000009751 Published online by Cambridge University Press

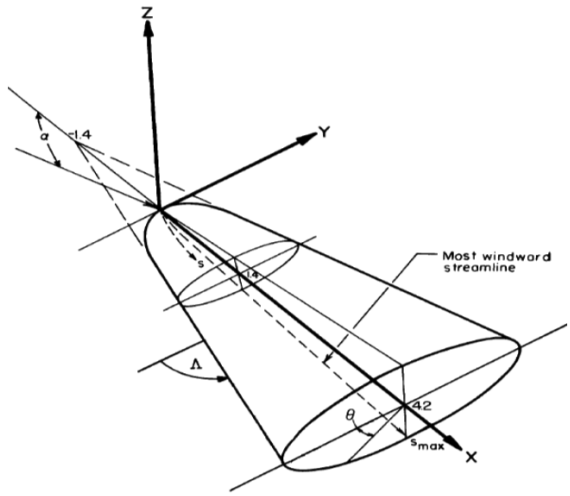


Figure 1. Double elliptic paraboloid and co-ordinate system[26].

as the ideal model for the present model. It is described by two elliptic paraboloidal profiles with smooth tangential junction at station $x = 1{\cdot}4$ inches from the leading edge.

The shape between the station $x = 0$ to $1{\cdot}4$ is given by the expression:

$$\frac{y^2}{(0{\cdot}4018x)} + \frac{z^2}{(0{\cdot}4018x)0{\cdot}5^2} = 1 \qquad \ldots (1)$$

And in between the junction $x = 1{\cdot}4$ to $4{\cdot}2$, the profile changes to:

$$\frac{y^2}{\left(\frac{x+1{\cdot}4}{\sqrt{13{\cdot}93}}\right)^2} + \frac{z^2}{\left(\frac{x+1{\cdot}4}{\sqrt{55{\cdot}76}}\right)^2} = 1 \qquad \ldots (2)$$

with smooth continuous surface junction at station $x = 1{\cdot}4$. The modified Newtonian expression for the pressure distribution on the body is given by the expression[25]:

$$C_p = \left(\frac{\gamma+3}{\gamma+1}\right)\left\{1 - \frac{\gamma+2}{\left(M_\infty(\gamma+3)\right)}\right\}\mathrm{Cos}^2\eta \qquad \ldots (3)$$

where η is the angle between the free stream velocity vector and the normal inner unit vector $\bar{n}$ to the ellipsoid surface, and is determined from the scalar product of the two vectors. The velocity vector is given by:

$$\bar{V}_\infty = -V_\infty(\bar{i}\,\mathrm{Cos}\,\alpha\,\mathrm{Cos}\,\beta + \bar{j}\,\mathrm{Sin}\,\beta + \bar{k}\,\mathrm{Sin}\,\alpha\,\mathrm{Cos}\,\beta) \qquad \ldots (4)$$

where $\bar{i}, \bar{j}$ and $\bar{k}$ are unit vectors along x, y and z directions shown in Fig. 1.The inward normal vector $\bar{n}$ is given by the equation:

$$\bar{n} = \bar{i}\,\mathrm{Cos}(n,x) + j\,\mathrm{Cos}(n,y) + \bar{k}\,\mathrm{Cos}(n,z) \qquad \ldots (5)$$

https://doi.org/10.1017/S0001924000009751 Published online by Cambridge University Press

where (n,x), (n,y) and (n,z) are the angles in between the vector $\bar{n}$ and the positive x, y and z directions. If the body surface may be described as function $\chi(x,y,z) = 0$, then

$$\mathrm{Cos}(n,\chi) = -\frac{\frac{\partial\chi}{\partial x}}{\sqrt{\left\{\left(\frac{\partial\chi}{\partial x}\right)^2+\left(\frac{\partial\chi}{\partial y}\right)^2+\left(\frac{\partial\chi}{\partial z}\right)^2\right\}}} \quad \ldots(6)$$

$$\mathrm{Cos}(n,y) = -\frac{\frac{\partial\chi}{\partial y}}{\sqrt{\left\{\left(\frac{\partial\chi}{\partial x}\right)^2+\left(\frac{\partial\chi}{\partial y}\right)^2+\left(\frac{\partial\chi}{\partial z}\right)^2\right\}}} \quad \ldots(7)$$

$$\mathrm{Cos}(n,y) = -\frac{\frac{\partial\chi}{\partial z}}{\sqrt{\left\{\left(\frac{\partial\chi}{\partial x}\right)^2+\left(\frac{\partial\chi}{\partial y}\right)^2+\left(\frac{\partial\chi}{\partial z}\right)^2\right\}}} \quad \ldots(8)$$

For the elliptic configuration shown in Fig. 1 at zero yaw angle ($\beta = 0$) and small angles of incidence α, the compound angle between free stream and the normal vector, η, at a station x is given by:

$$\mathrm{Cos}(\eta) = -\frac{\frac{\partial\chi}{\partial y}+\frac{\partial\chi}{\partial z}\alpha}{\sqrt{\left\{\left(\frac{\partial\chi}{\partial x}\right)^2+\left(\frac{\partial\chi}{\partial y}\right)^2+\left(\frac{\partial\chi}{\partial z}\right)^2\right\}}} \quad \ldots(9)$$

The steady solution is then perturbed using the unsteady shock expansion techniques proposed by Eggers[27] and applied by Zartarian *et al*[28] when the body is subject to certain pitch or translational motion schedules. The instantaneous height of a point on the body at a distance x from the vertex is given by:

$$h(x,t) = h(x_0,t) - (x\text{-}x_0)\vartheta(t) \quad \ldots(10)$$

where,

$$\vartheta(t) \equiv \alpha(t) + \mathrm{Sin}^{-1}\left(\frac{\dot{z}}{V_\infty}\right) \quad \ldots(11)$$

$$h(x,t) = \frac{1}{2}\ddot{z}\,t^2 - (x\text{-}x_0).\left[\alpha(t)+\frac{\ddot{z}}{V_\infty}t\right] \quad \ldots(12)$$

Considering a pitching motion only with a pitch rate of q (nose up) with, no other translational motion, i.e. $\theta(t) \equiv qt = \alpha(t)$ (if $\upsilon(0) = \alpha(0)$ and of course $\ddot{z} = 0$) so that

$$h(x,t) = -(x\text{-}x_0)qt \quad \text{and} \quad h(x,\tau(x)) = -(x\text{-}x_0)q\tau(x) \quad \ldots(13)$$

$$\therefore \frac{(\mathrm{d}h(x,\tau(x))}{\mathrm{d}x} = -q\left[\tau(x) + (x\text{-}x_0)\frac{(\mathrm{d}\tau(x)}{\mathrm{d}x}\right] \quad \ldots(14)$$

Starting from an instant t_0, time taken by a fluid element to traverse a distance, ds, along a path line is given by:

$$t = t_0 + \int_0^x \frac{\mathrm{d}s}{V} \quad \ldots(15)$$

which for a body with continuously changing profile is given by:

https://doi.org/10.1017/S0001924000009751 Published online by Cambridge University Press

$$t = t_0 + \int_0^x \frac{\sec\theta_0(x)\,\mathrm{d}x}{V} \qquad \ldots(16)$$

$\theta_0(x)$ refers to the local slope of the body at x and V corresponds to the local velocity. From Prandtl Meyer flow expansion from the velocity conditions at the nose (N) to any station x is given by:

$$V = \bar{V}_N \left\{1 - \frac{\theta_0 - \theta_N}{\sqrt{M_N^2 - 1}}\right\} \qquad \ldots(17)$$

Now making appropriate substitutions for the velocity terms and binomial expansion of the first term gives:

$$t = t_0 + \frac{\sec\theta_N}{\bar{V}_N}\int_0^x \left[1 + (\theta_0 - \theta_N).\mathrm{Tan}\,\theta_N\right]\left\{1 + \frac{\theta_0 - \theta_N}{\sqrt{\left(M_N^2 - 1\right)}}\right\}\mathrm{d}x \qquad \ldots(18)$$

which then results in:

$$\therefore t = \tau(x) = t_0 + \frac{\sec\theta_N}{\bar{V}_N}.\left\{x + (\mathrm{Tan}\,\theta_0 + \frac{1}{\sqrt{M_N^2 - 1}}.(\int_0^x \theta_0(x)\,\mathrm{d}x - x\theta_N)\right\} \qquad \ldots(19)$$

More explicitly for $x,\tau(x)$ then:

$$\frac{\mathrm{d}h(x,\tau(x)}{\mathrm{d}x} = -q_0\,t_0 - q\frac{\sec\theta_N}{V_N}\left\{\begin{matrix}(2x - x_0) + \left(\mathrm{Tan}\,\theta_0 + \dfrac{1}{\sqrt{M_N^2 - 1}}.(\int_0^x \theta_0\,(x)\mathrm{d}x - x\theta_N\right) + \\ (x - x_0).(\theta_0\,(x) - \theta_N)\end{matrix}\right\} \qquad \ldots(20)$$

And at $x = 0$,

$$\left[\frac{\mathrm{d}h(x,\tau(x))}{\mathrm{d}x}\right]_{x=0} = -q\left(t_0 - x_0\,\frac{\sec\theta_N}{\bar{V}_N}\right) \qquad \ldots(21)$$

Provided that terms of the order of, $\int_0^x(\theta_0(x) - \theta_N)^2\,\mathrm{d}x$, may be neglected compared to x for integral $n \geq 2$. Knowing that in the limits 0 to x:

$$\Delta\varepsilon_p(x) = \left[\mathrm{Tan}^{-1}\left\{\frac{\mathrm{d}h(x,\tau(x))}{\mathrm{d}x}.\mathrm{Sin}\varphi + \frac{\mathrm{d}R(x)}{\mathrm{d}x}\right\}\right]_{(0,x)} \qquad \ldots(22)$$

$$\Delta\varepsilon_p(x) = \mathrm{Tan}^{-1}\left\{\frac{\left|\frac{\mathrm{d}(x,\tau(x))}{\mathrm{d}x}\right|_{0,x}.\mathrm{Sin}\varphi + \left[\frac{\mathrm{d}R(x)}{\mathrm{d}x}\right]_{(0,x)}}{1 + \left[\frac{\mathrm{d}(x,\tau(x))}{\mathrm{d}x}\mathrm{Sin}\varphi + \frac{\mathrm{d}R(x)}{\mathrm{d}x}\right].\left[\frac{\mathrm{d}(x,\tau(x))}{\mathrm{d}x}\mathrm{Sin}\varphi + \frac{\mathrm{d}R(x)}{\mathrm{d}(x)}\right]_{x=0}}\right\} \qquad \ldots(23)$$

$\Delta\varepsilon_p(x)$, here has been measured in the initial x- r plane, i.e. the meridian plane at time $t = 0$ (when $\alpha = 0$ and $\dot{z} = 0$), and its sign has been chosen so as to be positive for a compression of the fluid and negative for an expansion.

Also consistent with the first-order approximations already made in the variables α, q, $\dot{z}$ and $(\theta_0(x) - \theta_N)$ — in fact, to second order – $\mathrm{Tan}\{\Delta\varepsilon_p(x)\} \approx \Delta\varepsilon_p(x)$; hence to same order, it can be shown that:

https://doi.org/10.1017/S0001924000009751 Published online by Cambridge University Press

$$\Delta\varepsilon_p(x) = (\theta_0(x) - \theta_N) + \mathrm{Cos}^2_N\varphi.\mathrm{Sin}\varphi \begin{Bmatrix} \left|\frac{d(x,\tau(x))}{dx}\right|_{0,x} \\ -2(\theta_0(x) - \theta_N).\mathrm{Tan}\varphi\frac{d(x,\tau(x))}{dx} \end{Bmatrix} \quad \ldots(24)$$

It can further be shown that the change in the inclination ($\Delta\varepsilon_p$) of a the projected path line of a particular fluid element between points (0,0,φ) and (x,$R(x)$,φ) on the body surface may be determined from the expansion of the above relationship:

$$\Delta\varepsilon_p(x) = (\theta_0(x) - \theta_N) + 2\vartheta\,(\theta_0(x) - \theta_N)\,\mathrm{Sin}\theta_N\,\mathrm{Cos}\theta_N\,\mathrm{Sin}\varphi - \frac{q}{\bar{V}_N}\,\mathrm{Cos}\theta_N\,\mathrm{Sin}\varphi.$$
$$\begin{Bmatrix} 2x + \mathrm{Tan}\theta_N.\left[\int_0^x \theta_0(x) - \theta_N)\,dx - (x - x_0).(\theta_0(x) - \theta_N\right] \\ + \frac{1}{\sqrt{M_N^2 - 1}}.\left[\int_0^x \theta_0(x) - \theta_N)\,dx - (x - x_0).(\theta_0(x) - \theta_N\right] \end{Bmatrix} \quad \ldots(25)$$

Thus the unsteady pressure distribution beyond a reference point chosen where the supersonic flow conditions are first met will be given by the expression:

$$\frac{p(x,\alpha,t)}{p(x,\alpha)} = 1 + \frac{\gamma M_x^2)}{\sqrt{M_{x\text{-}1}^2}}.\Delta\varepsilon_p \quad \ldots(26)$$

The steady component of pressure distribution on the surface of the elliptic body $\chi(x,y,z)$ is given by:

$$\frac{p(x,\alpha)}{p_\infty} = \frac{\gamma M_\infty^2}{2}.\left(\left(\frac{\gamma+3}{\gamma+1}\right)\left\{1 - \frac{\gamma+2}{M_\infty(\gamma+3)}\right\}\frac{\left(\frac{\partial\chi}{\partial x} + \frac{\partial\chi}{\partial z}\alpha\right)^2}{\left\{\left(\frac{\partial\chi}{\partial x}\right)^2 + \left(\frac{\partial\chi}{\partial y}\right)^2 + \left(\frac{\partial\chi}{\partial z}\right)^2\right\}} + 1\right) \quad \ldots(27)$$

The unsteady pressure coefficient along the body may be obtained from the last two equations as:

$$C_p = \frac{2}{\gamma M_\infty^2}\left\{\frac{p(x,\alpha,t)}{p(x,\alpha)}.\frac{p(x,\alpha)}{p_\infty} - 1\right\} \quad \ldots(28)$$

As noted in the definition of the static and stability derivatives, there are no translation displacements or other velocities ($\dot{z}$, $\dot{\boldsymbol{z}}$) considered in present analysis. Similarly the $\dot{\alpha}$ contribution following the analysis due to Ericsson[29] is assumed to contribute negligible contribution to the dynamic stability parameter $Cm_{\dot{\vartheta}}$.The static and dynamic pitching moment derivatives around the body with two axes of symmetry are thus given by:

$$Cm_\alpha = -\frac{l}{S\,l}\left\{\begin{array}{l} \int_{M_\infty^2}^{l}\int_0^{2\pi}\frac{\partial Cp}{\partial\alpha}R(x,y,z)\,\mathrm{Cos}\,(n,z)\,l(x)\,\mathrm{Sin}\varphi\,d\varphi\,dx \\ -\int_0^{2\pi}\int_0^{l}\frac{\partial Cp}{\partial\alpha}R(x,y,z)\,\mathrm{Cos}(n,x)\,l(y)\,\mathrm{Sin}\varphi\,d\varphi\,dx \end{array}\right\} \quad \ldots(29)$$

$$Cm_{\dot{\vartheta}} = -\frac{2V_\infty}{S\,l}\left\{\begin{array}{l} \int_0^{l}\int_0^{2\pi}\frac{\partial Cp}{\partial q}R(x,y,z)\,\mathrm{Cos}\,(n,z)\,l(x)\,\mathrm{Sin}\varphi\,d\varphi\,dx \\ -\int_0^{2\pi}\int_0^{l}\frac{\partial Cp}{\partial q}R(x,y,z)\,\mathrm{Cos}(n,x)\,l(y)\,\mathrm{Sin}\varphi\,d\varphi\,dx \end{array}\right\} \quad \ldots(30)$$

The expression for $\partial\Delta\varepsilon_p / \partial\alpha$ and $\partial\Delta\varepsilon_p / \partial q$ needed in the evaluation of $Cm_{\dot{\vartheta}}$ may be obtained by an appropriate differentiation of the above equation for $\Delta\varepsilon_p$.

https://doi.org/10.1017/S0001924000009751 Published online by Cambridge University Press

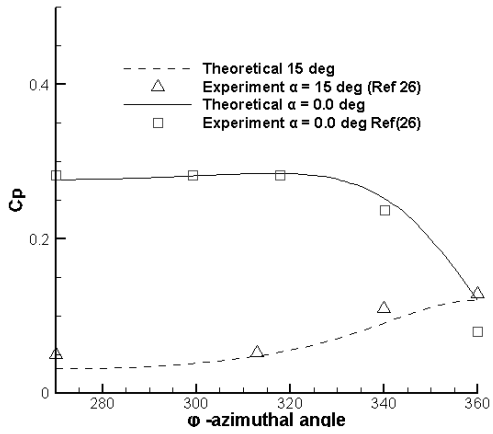


Figure 2. C_p vs φ at M_∞ = 4·7, x = 2·6in.

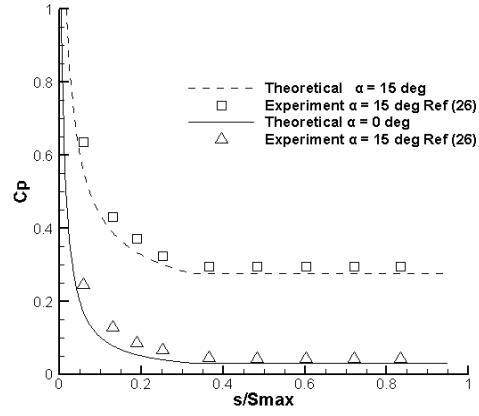


Figure 3. C_p vs distance along body (most windward station).

3.0 DISCUSSION OF RESULTS

Dynamic stability derivatives as obtained in this paper depend to a large extent upon the steady pressure field which is then perturbed using the shock expansion method. Towards this end then, the steady pressure distribution was examined for accuracy in both axial and azimuth directions. Figure 2 shows a comparison of pressure coefficient plotted against the azimuthal angle φ increasing from the most wind ward generator (φ = 270˚) towards the horizontal location (φ = 360˚) at angles-of-attack α = 0 and 15˚. Figure 3 records the comparison of *Cp* against the distance along the curved surface at the most wind ward generator again at α = 0 and 15˚. Note the high pressure gradients near the stagnation region are caused by the high curvature of the shock in the vicinity of the nose. The agreement between the present computed values and the experiment by Kussoy[26] is quite satisfactory.

The dynamic stability data for the blunt elliptic body shown in Fig. 1 is virtually non-existent. Only some minimal data was found for the pointed elliptic cone in Ref. 26. The above method was then run on the pointed ellipsoid with foci lengths (a/b = 0·75). The equation for the pointed elliptical configuration $z^2/A^2 + y^2/B^2 = 1$ with local radius at any location x is given by: $R = \sqrt{((a^2 x^2 \text{Cos}^2)\theta + b^2 x^2 \text{Sin}^2\theta)}$. The dynamic stability derivative $Cm_{\dot{\vartheta}}$ for this pointed elliptic cone when plotted against the blunt cone from Fig. 1 as shown in Fig. 4. In most of the following comparisons of dynamic stability and static stability, the data for a blunt cone (R_N/R_B = 0·3) from Ref. 18 is provided only to give an idea of the dynamic stability measure, however, the pointed ellipsoid results do provide a direct comparison against a corresponding sharp body.

As observed in Fig. 4, the pointed ellipsoid results remain consistently higher than corresponding blunt ellipsoid. The ellipsoid with the major axis in vertical configuration seem to be more damped than the results for the pointed ellipsoid cone sitting flat with major axis in vertical configuration. This trend has already been noted[17,18] between the pointed and blunt right cones. Devan's results[30], as shown here, were only available for the supersonic Mach number range from M_∞ = 1·46 to about M_∞ = 4. No such data was available for higher Mach numbers. At the lower end of the Mach number range shown here, the present results for the pointed elliptical cone with the same aspect ratio run comfortably into the results from Ref. 30.

https://doi.org/10.1017/S0001924000009751 Published online by Cambridge University Press

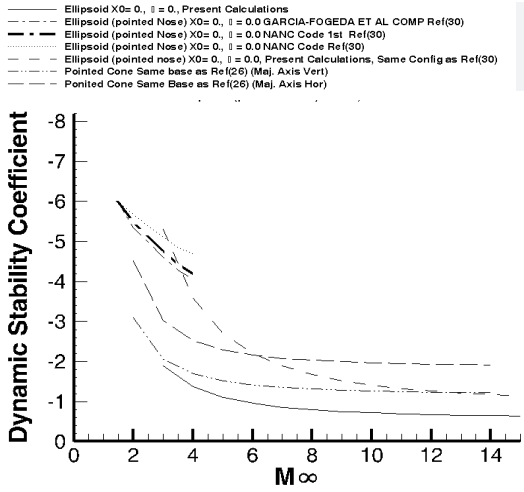


Figure 4. $Cm_{\dot{\vartheta}}$ vs Mach number M_∞.

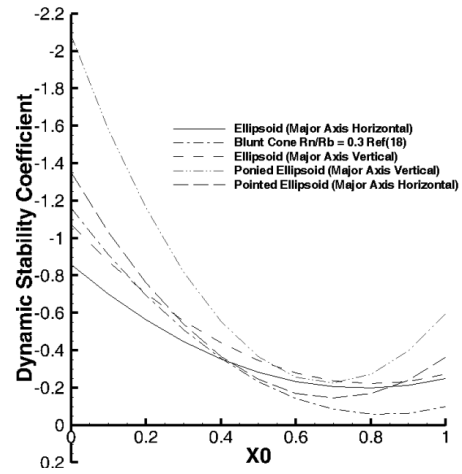


Figure 5. $Cm_{\dot{\vartheta}}$ vs X_o with M_∞= 7·0.

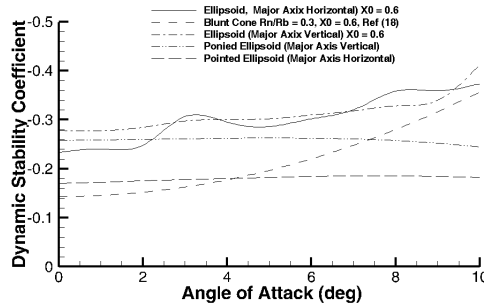


Figure 6. $Cm_{\dot{\vartheta}}$ vs α, X_o = 0·6, M_∞= 7·0.

Figure 5 shows the damping in pitch dynamic stability derivative $Cm_{\dot{\vartheta}}$. for the blunt ellipsoid shown in Fig. 1, plotted against the axis of oscillation position x_0 for the free stream Mach number M_∞ = 7·0. In absence of any experimental data for this case, the results for a blunt cone R_N/R_B = 0·3 of equivalent length are also included. For a further measure of validation, the results for the same ellipsoid with axis rotated through 90 degrees (major axis vertical) are also shown. As a matter of direct comparison, the results for pointed ellipsoids are also shown. The pointed elliptic cone, when standing on its major axis, displays the largest - $Cm_{\dot{\vartheta}}$ values for all x_0 locations. The same cone when flat on elliptic axis too shows more damping except for the range $0{\cdot}4 \le x_0 \le 0{\cdot}875$ where they dip below the corresponding blunt ellipsoids.

The blunt right cone remains decidedly less damped than all other configuration for $x_0 \ge 0{\cdot}4$. The minimum dynamic stability for all configurations tested here is found in the range $0{\cdot}65 \le x_0 \le 0{\cdot}85$.

The dynamic stability for above cases was also examined against the angle-of-attack, α. It must be noted here that the pressure distribution for finite angles of attack is again adopted from Newtonian concepts which may hold good for small angles-of-attack of up to about $\alpha \le 5°$ and may not be as accurate for higher angles-of-attack. The results for a free stream value of M_∞ = 7·0 and axis of oscillation position X_o = 0·6 are shown in Fig. 6. In absence of any other experimental data for this configuration, the results are compared against an 'equivalent' blunt cone. It is observed that

https://doi.org/10.1017/S0001924000009751 Published online by Cambridge University Press

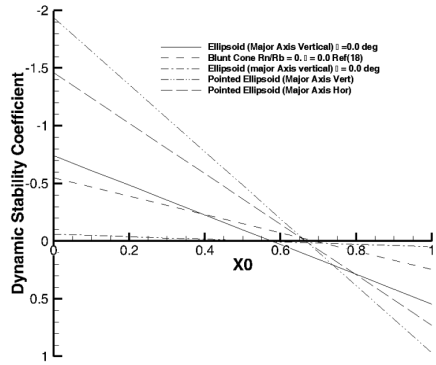


Figure 7. Cm_{α} vs x_o, α = 0·0˚, M_{∞} = 7·0.

in all cases the dynamic stability increases with angle-of-attack, with the ellipsoid in both orientations remaining consistently above the blunt cone results. It is interesting that the ellipsoid with the major axis in the horizontal position appears to show a couple of bulges near angles-of-attack values of α = 3˚ and 8˚. The pressure field from blunt configurations are more sensitive to nose especially at finite α's, and hence a more noticeable effect on $Cm_{\dot{\vartheta}}$ with α.

The pressure field near the ellipsoid apexes (major axis horizontal) must contain some fattening which translates into these bumps. However, when the ellipsoid is already in the vertical direction these effects are hidden by producing an apparent larger local angle-of-attack.

For the sake of completeness, the static stability derivative Cm_{α} results for the blunt ellipsoid as shown in Fig. 1, are reported in Fig. 7. The pointed ellipsoids for both configurations (major axis horizontal and vertical) display more static damping than the corresponding blunt ellipsoids for $x_0 \leq 0{\cdot}7$ The static stability for the pointed elliptical cones have a neutral point at $x_0 = 0{\cdot}7$. Blunt ellipsoid too displays a decreasing static stability trend against the axis of oscillation position, passing through a neutrality point $Cm_{\alpha} = 0$ at $x_o \approx 0{\cdot}6$. The graph shows a more static damping for a blunt ellipsoid compared to an equivalent blunt cone ($R_n/R_b = 0{\cdot}3$) up until $x_o = 0{\cdot}4$, beyond which point the trend is interchanged.

4.0 CONCLUSION

In absence of any reliable experimental data on blunt elliptic cones, the present results could only be compared against available data on pointed elliptic cones from literature, or as a simple point of reference, the results are qualitatively studied against 'equivalent' blunt cones. For elliptic bodies it is observed in all configurations that when standing on the larger axis ($a > b$), the body appears to be more damped. It is quite possible that, when sitting horizontally, it produces a larger blunting effect in pitch and is consequently less damped.

The dynamic stability derivatives for the blunt ellipsoid calculated using the present method show satisfactory trends when compared against available data in literature (which is very scarce) or when compared against blunt cone results.

It appears that the pointed elliptic cone would be dynamically more stable than an equivalent blunt elliptic cone; a result which appears to mimic the comparison between pointed and blunt axisymmetric cones. The pointed body in all cases would suffer from the same high heat transfer effects in all cases.

https://doi.org/10.1017/S0001924000009751 Published online by Cambridge University Press

REFERENCES

1. HUI, W.H. Stability of oscillating wedges and caret wings in hypersonic and supersonic flows, *AIAA J*, 1969, **7**, 1524–1530.
2. HUI, W.H. Interaction of a strong shock with Mach waves in unsteady flow, *AIAA J*, 1969, **7**, 1 605–1607.
3. HUI, W.H. Large-amplitude slow-oscillation of wedges in inviscid hypersonic and supersonic flows, *AIAA J*, 1970, **8**, 1530–1532.
4. HEMDAN, H. Similarity solutions for oscillating pointed-nosed slender axisymmetric bodies – Part II: Curved bodies, *Acta Astonautica*, 2001, **49**, No. 11, pp. 611–626.
5. HOBBS, R.B. Results of experimental studies on the hypersonic dynamic stability characteristics of a 10° cone at M - 20, May 1964, General Electric ATDM 1:37.
6. WELSH. C.J., WINCHENBACH, G.L. and MADAGAN, A.N. Free-flight investigation of the aerodynamic characteristics of a cone at high Mach numbers, *AIAA J*, 1970, **8**, No. 2. , pp. 294-300.
7. BRONG, E.A. The flow field about a right circular cone in unsteady flight, 1965, AIAA Paper 65-398, San Francisco, CA, USA.
8. RIE, H., LINKIEWICZ, B.A. and BOSWORTH, F.D. Hypersonic Dynamic Stability, Part III, Unsteady Flow Field Program, Jan 1967, FDL-TDR-64-149, Air Force Flight Dynamics Lab., Wright-Patterson Air Force Base.
9. VAN DYKE, M.D. A study of hypersonic small disturbance theory, 1954, NACA Report 1194.
10. BUSEMANN, A. Flussigkeits –und Gasbewegund, handworterbuch der Naturwissenschaften, Zweite Auflage (Gustav Fischer, Jena), 1933, pp 257-277.
11. PROBSTEIN, R.F. and BRAY, K.N.C.A. Hypersonic similarity and the tangent cone approximation for the un yawed bodies of revolution, *J Aeronaut Sci*, Jan 1958, **22**, no. 1, pp 66-68.
12. LIGHTHILL, M. Oscillating airfoils at high Mach number, *J Aeronaut Sci*, 1953, **20**, No. 6, , pp. 402–406.
13. ASHLEY, H. and ZARTARIAN, G. Piston theory - A new aerodynamic tool for the aeroelastician, *J Aeronaut Sci*, 1956, pp 1109–1118.
14. KHALID, M. and EAST, R.A. Stability derivatives of blunt cones at high Mach Numbers, *Aeronautical Q*, Nov 1979, **30**, pp-559-590.
15. TAYLOR, G.I. The formulation of a blast wave by a very intense explosion, *Proc Roy Soc (a)*, 1952, **201**, 159 - 186.
16. CHERNYI, G.G. *Introduction to Hypersonic Flow*, (translated from Russian by PROBSTEIN, R.F.), 1961.
17. KHALID, M. and EAST R.A. High Mach number dynamic stability of pointed cones at angles of attack, *AAIA J*, October 1980, **18**.
18 KHALID, M. Stability derivatives of blunt cones at high Mach numbers, *Aeronaut J*, 1992, **30**, pp 559 - 570.
19. KHALID, M. Viscous contribution to the high Mach number damping in pitch of blunt slender cones at small angles of attack, *Aeronaut J*, February 1995, pp 69-74.
20. RAMUSSEN M.L. and LEE, H.M. Approximation for hypersonic flow past slender elliptic cone, 1979, AIAA Paper 79-0364, 17th AIAA Aerospace Meeting, New Orleans, January 1979.
21. ERICSSON L.E. Technical evaluation report on the Fluid Dynamics Panel Symposium on Dynamic Stability Parameters, 1979, AGARD AR-137.
22. HAYES, W.D. and PROBSTEIN, R.F. *Hypersonic Flow Theory*, 1955, Academic Press, New York, USA.
23. BERTRAM, M.H. Boundary-layer displacement effects in air at Mach numbers of 0.8 and 9.6, 1957, NACA Technical Note no. 4133 ()
24. KENDALL, J.M. An experimental investigation of leading edge shock wave – boundary layer interaction at Mach 5.8, *J Aeronaut Sci*, 1957, **24**, pp 47-56.
25. LEES, L. Hypersoic Flow, June 1955, IAS Reprint No. 554.
26. KUSSOY, M. Local pressure distribution on a blunt delta wing for angles of attack up to 35° at Mach Numbers 3.4 to 7, NASA Technical Note D-1554.
27. EGGERS, A.J. On the calculation of flow about objects travelling at high supersonic speeds, 1952, NACA TN 2811.
28. ZARTARIAN, G., HSU, P.T. and ASHLEY, H. Dynamic air loads and aero elastic problems at reentry Mach numbers, *J Aeronaut Sci*, March 1961, **28**, (3).
29. ERICSSON, L.E., $\dot{\alpha}$ effects are negligible in hypersonic flow - fact or fiction, 1968, 19th International Congress of the Aeronautical Federation, New York, USA.
30. DEVAN, L. Non-axisymmetric body supersonic inviscid dynamic derivative prediction, 1989, NSWC TR 89-99, Naval Surface Warfare Centre.

https://doi.org/10.1017/S0001924000009751 Published online by Cambridge University Press